Cytometry 11:80–93 (1990)

Multivariate Chromosome Analysis and Complete Karyotyping Using Dual Labeling and Fluorescence Digital Imaging Microscopy

Donna J. Arndt-Jovin and Thomas M. Jovin

Department of Molecular Biology, Max Planck Institute for Biophysical Chemistry, Federal Republic of Germany

Received for publication June 6, 1989; accepted June 28, 1989

The combination of multiple dye-DNA interactions, a fluorescence digital imaging system with a scientific CCD camera, and multivariate image analysis allows the rapid karyotyping of fluorescent human metaphase chromosome spreads. Chromosomes are stained with the bisbenzimidazole dye Hoechst 33342 and chromomycin A_3, a dye pair used frequently in bivariate flow analysis and sorting of metaphase chromosomes in suspension. The use of ratio functions involving the total and peak intensities of the two dyes provides increased resolution of the karyotype in the microscope, and it can be anticipated that the same approach could lead to improved performance with flow systems as well. High pass filtering with a Laplace operator yields characteristic banded images of the individual chromosomes, even with total fields that are less than 200 pixels on a side.

Key terms: CCD camera, bis-benzimidazole, chromomycin, cytogenetics

Sam Latt's career exemplified the productive interface between medical problems (in particular, human genetics) and biophysical techniques. The application of fluorochromes in staining metaphase chromosomes by Caspersson and coworkers (9) revolutionized karyotype identification and, thereby, the field of human genetics. Latt identified energy transfer and quenching as the predominant determinants of chromosome banding patterns (4,6,22,29), thus providing a framework by which existing data on chromosome karyotyping could be evaluated. He introduced the use of the bisbenzimidazole dyes for chromosome staining and investigated their physico-chemical properties on normal and bromodeoxyuridine (BrdUrd)-substituted DNA (20,25,26). His papers on increased contrast in chromosome banding due to dye pair-DNA interactions (19,21,23,24,29) assisted in the evaluation of various genetically inherited translocations.

The original studies of Caspersson and coworkers demonstrating that most human chromosomes have a unique DNA content were the basis of the first quantitative cytochemical determinations (7) as well as of existing classification schemes based on UV absorption (27). The extension of karyotyping to flow cytometry utilized fluorochrome staining protocols which had proven effective in the quantitation of cellular DNA (2,11,13,17). Initial univariant flow karyotypes (8,32) with insufficient resolution were supplanted by bivariant flow karyotypes (14,18) based on the dye interaction studies of Latt and coworkers and the implementation of dual laser beam flow cytometers (31). Although all of the human chromosomes except 9–12 and 14 and 15 can generally be distinguished by flow karyotyping, detection of clinically significant chromosomal abnormalities has been hindered by problems related to the preparation of high-quality chromosome suspensions from small numbers of cells and of homolog variations between individuals. Slit-scanning flow cytometry can provide additional resolution (5, 10, and references therein), but it is still imperative to perform morphological observations with a microscope in order to substantiate the presence and nature of deviant chromosomes. Thus, the present-day cytogeneticist relies on banding techniques and on manual or semiautomatic systems for karyotyping (28).

High-resolution CCD cameras installed on digital imaging microscopes (DIM) provide a means for linear, stable, and sensitive fluorescence imaging (1,3,15,16). We demonstrate in this report that the use of dye pairs for the staining of chromosomes initiated by Latt can be combined with fluorescence DIM (FDIM) to generate bivariate karyotypes from chromosome spreads similar to those obtained with flow cytometers (12,14). In addition, we find that new functional combinations of the fluorescence signals can be used to derive multivariate distributions with characteristic features that

distinguish all but two of the human chromosomes. Digital enhancement techniques applied to the images accentuate the weak banding patterns of bis-benzimidazole 33342 and chromomycin A_3, thereby establishing a morphological substantiation of the chromosome assignments. It is postulated that further implementation of Latt's enhanced fluorochrome banding techniques can provide the means for automated karyotyping using FDIM.

MATERIALS AND METHODS

Chromosomes

Chromosome spreads were prepared from peripheral blood lymphocytes of one normal male individual by established procedures (30). After dehydration and air drying, the spreads were stained and mounted in 4 μM bis-benzimidazole 33342 (BBI) and 12 μM chromomycin A_3 (CA3) in a 5 mM KPO_4 (pH 8.0), 75 mM KCl, 10 mM $MgCl_2$ buffer. For quinacrine banding, spreads were stained first with a solution of 20 mg/ml quinacrine-HCl in water, washed with water, McIvaine's buffer, and water following the protocol of Sahar and Latt (29). After imaging, destaining was achieved by immersion of the slides in fixative (acetic acid:ethanol, 1:3) followed by staining with BBI and CA3 as given above. (It should be noted that since destaining by this procedure was not complete, the quantification of the spreads subsequently stained with BBI and CA3 was not as good as that of preparations which had not been exposed to quinacrine.

Digital Camera, Microscope, and Image Acquisition

A Zeiss Universal microscope was equipped with a Photometrics (Tucson, Arizona) CH220 Camera incorporating a thermoelectrically cooled CSF-Thomson TH7882CDA CCD with 384 × 576 23 μm^2 pixels coated with a downconverter (Metachrome II) for improved blue response. The camera has a dark noise of 0.6 count/s, a dynamic range of 0–16,383 counts (14-bit ADC), and a linearity of >99%. A 40× Neofluar oil immersion, NA 0.9 objective and a Plan-Neofluar 63× oil immersion, NA 1.3 objective were used together with an Optovar zoom (1.25×). With the 40× and 63× objectives, a pixel corresponded to 0.28 μm and 0.18 μm in the object plane, respectively. The excitation source was a 100-W Hg lamp attenuated by a quartz 0.1 neutral density filter. BBI images (Im_1) were taken with a 12 nm halfwidth (HW) bandpass excitation filter at 365 nm, combined with a 395 nm dichroic and 418 nm longpass emission filter. CA3 (Im_2) and quinacrine (Im_3) images were taken with an 8 nm HW bandpass excitation filter at 436 nm, combined with a 460 nm dichroic and a 470 nm longpass emission filter. Fluorescence images were acquired with an integration time of 5 s during which no perceptible bleaching occurred and resulted in images with peak intensities of 6,000–12,000 counts. Local preprocessing of the images was performed with a Photometrics CC200 camera controller. A background image of the dye solution was taken for the same exposure time and subtracted from each image. Flat field corrections for inhomogeneity in the excitation and detection fields were made by division with an image generated with a fluorescent uranium glass (Schott GG17). Images were then transferred to a DEC MicroVaxII for processing.

Image Processing

A package of analysis programs was developed using TCL-Image V4.2, a system for image processing developed at the Delft Center for Image Analysis and distributed by Multihouse TSI, Amsterdam. The Photometrics digital camera control unit was coupled to a central DEC MicroVax II system operating under VMS V4.7. Standard TCL-image files with short word (16 bit) pixels were written first on a central magnetic drive unit, then stored on optical disks (Maxtor RXT-800S). A series of macros implemented with standard TCL-image commands performed the following functions:

Image centering and registration. A "center of mass" was defined for the entire grey value image and used as a displacement vector approximately to center the metaphase spread in the destination field. This procedure automatically achieved a satisfactory registration of the images (Im_1, Im_2, Im_3) corresponding to the fluorescence signals from the various dyes.

Segmentation. A three-stage procedure was adopted based upon successive thresholding. An initial "soft" threshold set at 5–10% of the maximal pixel value in the image defined a field encompassing all chromosomes and eliminating some of the background. The resultant binary mask was smoothed and small defects filled. A second mask was established by thresholding at a 30% (of maximum) level, a value achieved by parts of all chromosomes. Isolated objects (single and multiple chromosomes) were labeled and those with less than 5% of the total area rendered "immortal" by placing a high pixel value at their center of mass. (This procedure assured that the smaller chromosomes were not obliterated in the next step of segmentation.) The final mask was generated by thresholding in the 40–60% range (an adjustable parameter). The regions so defined were used to generate an exoskeleton demarcating the objects (chromosomes) and the final labels were generated from the union with the original background mask. In this manner, the attempt was made to define regions in which all the light (in-focus, out-of-focus) corresponding to the individual chromosomes would be collected, thereby ensuring optimal quantitation of the fundamental fluorescence parameters used for analysis: total emission ($S_{i,k} = \Sigma I_{i,j}$) where i designates the signal type, j is an index over the object pixels in the segmentation mask, and k is the index of chromosomes (by type); and the peak intensity $M_{i,k}$ of chromosome i,k. Both of these quantities were normalized by the cumulative intensity within the composite mask corresponding to the entire metaphase spread ($\Sigma S_{i,k}$).

Initial evaluation of another segmentation procedure based on boundary detection from determinations of gradients has demonstrated improved discrimination between adjoining chromosomes and intrachromosomal constrictions and will be reported on elsewhere.

Object (chromosome) characterization. Each label corresponding to the segmented chromosomes was used to define subimages within which a number of quantities were evaluated: $I_{i,j}$, $S_{i,k}$, $M_{i,k}$; moments and statistics related to the intensity distribution function; a "moment of inertia" (a distance parameter characterizing the spatial distribution of intensity); and less useful parameters derived solely from the binary masks, e.g. areas and contour lengths. These quantities were written into tabulated file lists for further processing and plotting, the latter using commercial programs on an Apple Macintosh II.

Utilities. Routines were developed for labeling (numbering) segmented images, for removing labeling inconsistencies between the various masks (corresponding to the I_i), for performing I/O, for displaying images or correlated parameters according to different formats, and for normalizing individual chromosome subimages by linear contrast stretching or by histogram equalization. These operations were carried out on (i) the original images, (ii) the images consisting of positive values resulting from application of the 3 × 3 Laplace gradient operator; and (iii) the sum of (i) and (ii). The images specificied in (ii) provided superior definition for visual karyotyping according to characteristic intensity distributions and banding patterns, especially with the BBI stain.

RESULTS

Image Processing

After determination of the labeled masks by segmentation, each set of dual (BBI, CA3) images was processed to generate an "image gallery": A) the original image; B) the result of a Laplace edge detector applied to image A, clipped to positive values; and C) the sum of images A and B, i.e., a high-pass filter operation. Images AN, BN, and CN were generated from A, B, and C, respectively, by normalizing each chromosome individually to the same range (0–10,000, or, for display purposes, 0–255). These normalized images provide the best visual impression of chromosome size, morphology, and banding inasmuch as they compensate for the greater than twofold differences in peak intensities (see below). Taken together, the members of the image gallery greatly facilitate assignment of the chromosomes by operator inspection. Quantitative analyses, however, were performed solely on the original images A, except for one test case in which a prior normalization to 8 bits was carried out. The image galleries corresponding to data acquired with the 40× objective are shown in Figures 1 and 2. The high-pass filtering provides a significant increase in contrast such that the chromatids and distinctive bands become perceptible, even though the total field is encompassed in a square with only 200 pixels on a side. The images obtained with the 63× objective (not shown) were correspondingly larger and more detailed but less reproducible from the standpoint of quantification, as discussed below.

Chromosome Assignment

Chromosome spreads were labeled with quinacrine and several metaphase plates localized and imaged. The slides were then destained in fixative and restained with BBI and CA3. The assignments used below were made by karyotyping of the quinacrine stained plates with the help of a trained cytogeneticist and correlation with the BBI and CA3 image galleries. The chromosomes in other metaphase sets were identified by comparing BBI and CA3 DIM images with those of the completely karyotyped spreads.

Intensity Parameters Correlated to Chromosome Assignment

The fluorescence signals from two metaphase spreads taken with the 40× objective and with the 63× objective are correlated to the chromosome assignment in panels A–C of Figures 3 and 4, respectively. Panels A depict the normalized total emission (relative fluorescence) from each homolog and for each dye $S_{1,k}$ (□) and $S_{2,k}$ (■). The data obtained at the two magnifications are in excellent agreement and demonstrate that the normalized fluorescence signals provide a measure of the chromosome DNA content and composition irrespective of magnification or chromosome condensation. The normalized maximal pixel intensities (relative peak fluorescence) in each chromosome homolog from both dyes, $M_{1,k}$ (□) and $M_{2,k}$ (■), are plotted in panels B. Significant differences in the homologs and between the two plates are seen since this parameter is sensitive to chromosome condensation and to the system magnification, i.e., pixel resolution. However, if we plot instead the ratio of the total emission, $S_{1,k}/S_{2,k}$ (□), and the ratio of the peak values, $M_{1,k}/M_{2,k}$ (■), for each chromosome, distinctive and reproducible patterns emerge (panels C). Thus, a characteristic set of

FIG. 1. Bis-benzimidazole 33342 (BBI) fluorescence digital images of a metaphase chromosome plate, original and after digital filtering. **A:** Original grey scale image normalized to 256 levels for display. **B:** Image of positive values after Laplace gradient operation using a 4-connectivity mask on the original image (A). **C:** Image generated by addition of images A and B. **AN–CN:** Images generated from A–C, respectively, by normalization of each individual chromosome to 256 grey levels. File: s11718.

FIG. 2. Chromomycin A_3 (CA3) fluorescence digital images of the same metaphase chromosome plate as in Figure 1. Key as in Figure 1. The arrows in panel **CN** point to the very bright satellites of chromosome pair 9. The monitor was adjusted for maximal contrast in the remainder of the karyotype such that the other regions of chromosome 9 (visible in panel **C**) are no longer apparent. (Note: this figure appears on page 84.)

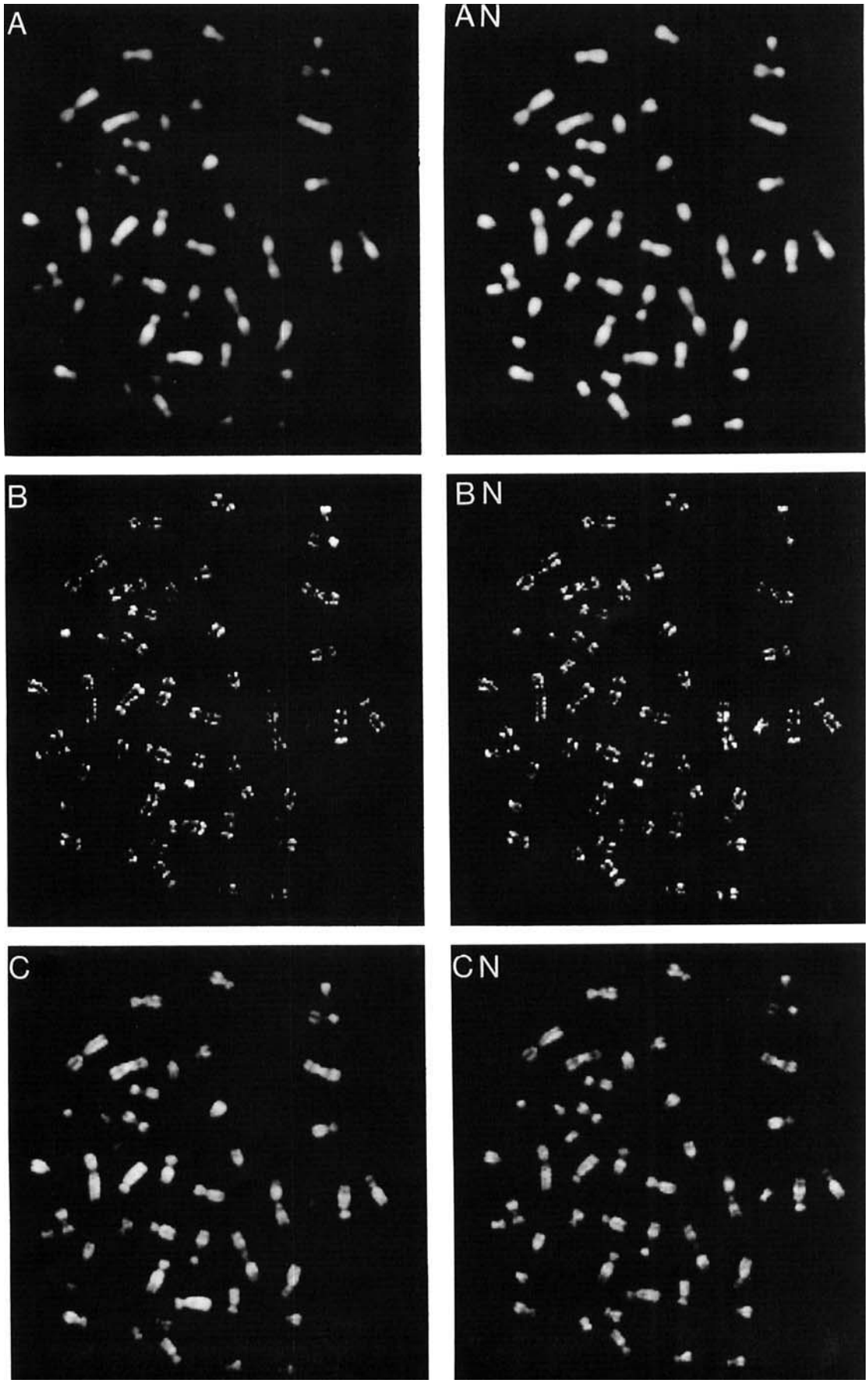

FIG. 1.

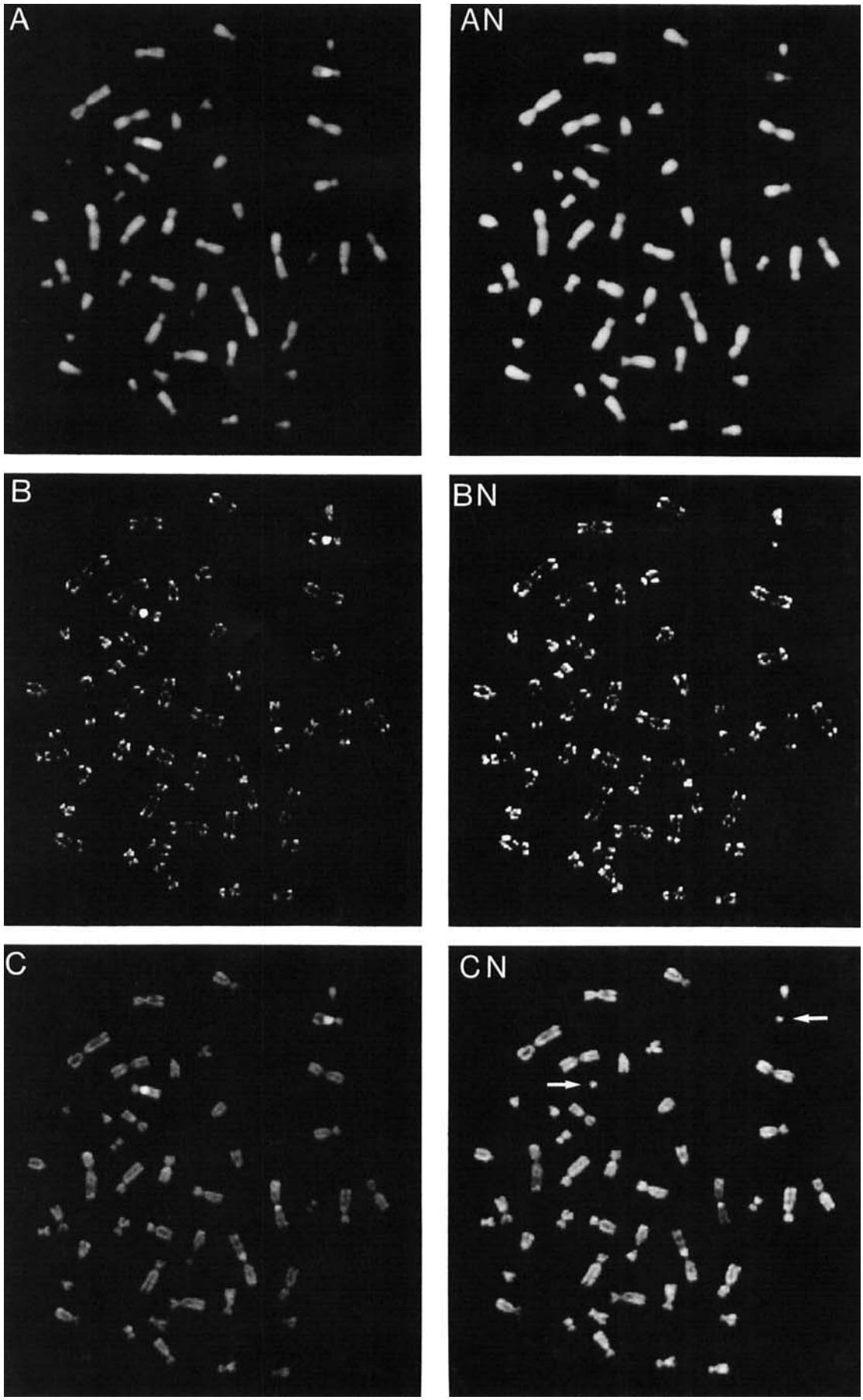

FIG. 2.

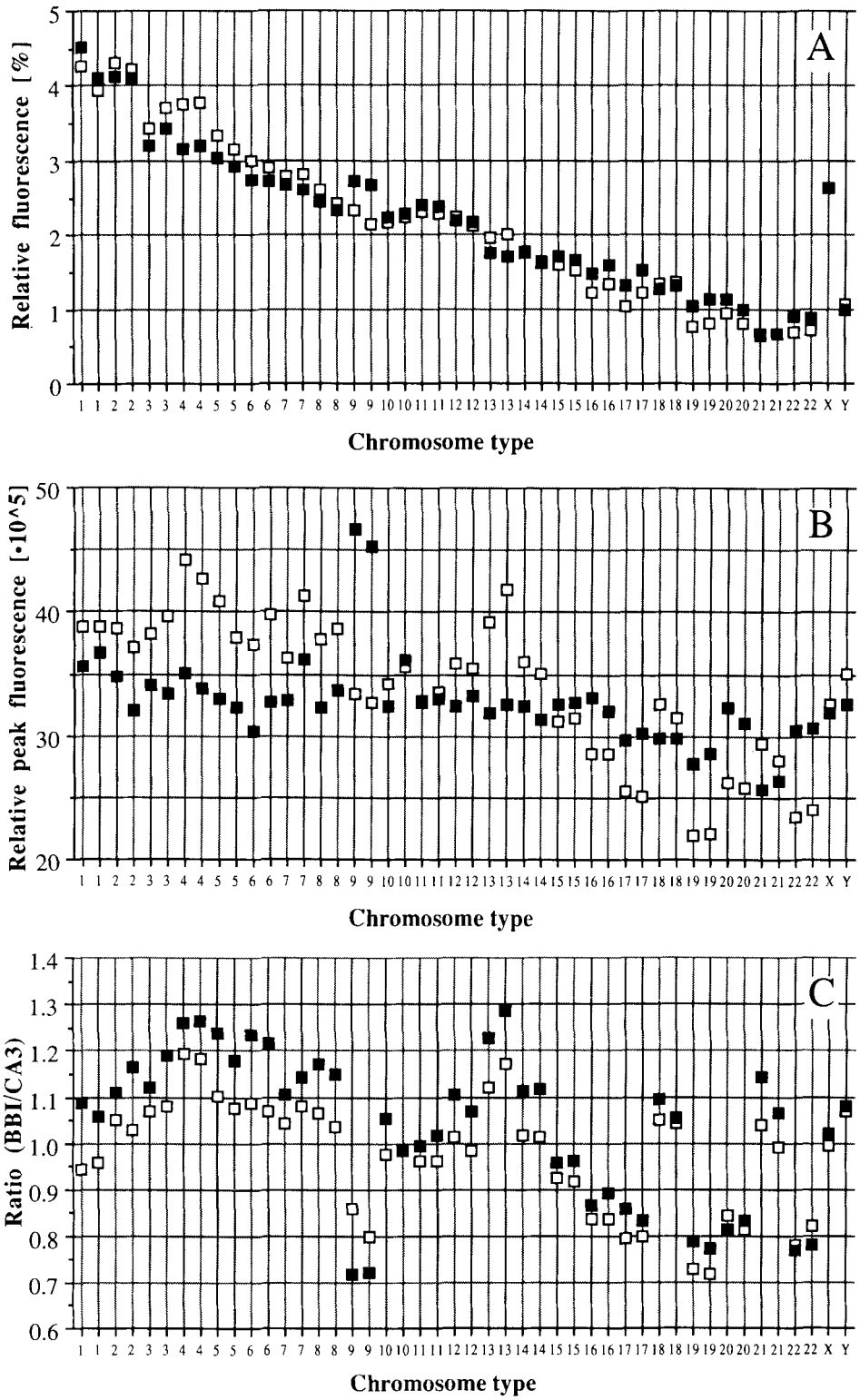

FIG. 3. Analyzed fluorescence intensity data for BBI and CA3 images correlated to the chromosome assignment. Measurements with the 40× objective (Figs. 1, 2). **A:** Normalized total emission plotted against chromosome number for each homolog: BBI, $S_{1,k}$ (□); CA3, $S_{2,k}$ (■). **B:** Maximum pixel intensity in each chromosome homolog: BBI, $M_{1,k}$ (□); CA3, $M_{2,k}$ (■). **C:** Ratio (BBI/CA3) of the total emission and of the normalized peak values for each chromosome homolog: $S_{1,k}/S_{2,k}$ relative fluorescence (□); $M_{1,k}/M_{2,k}$ relative peak fluorescence (■).

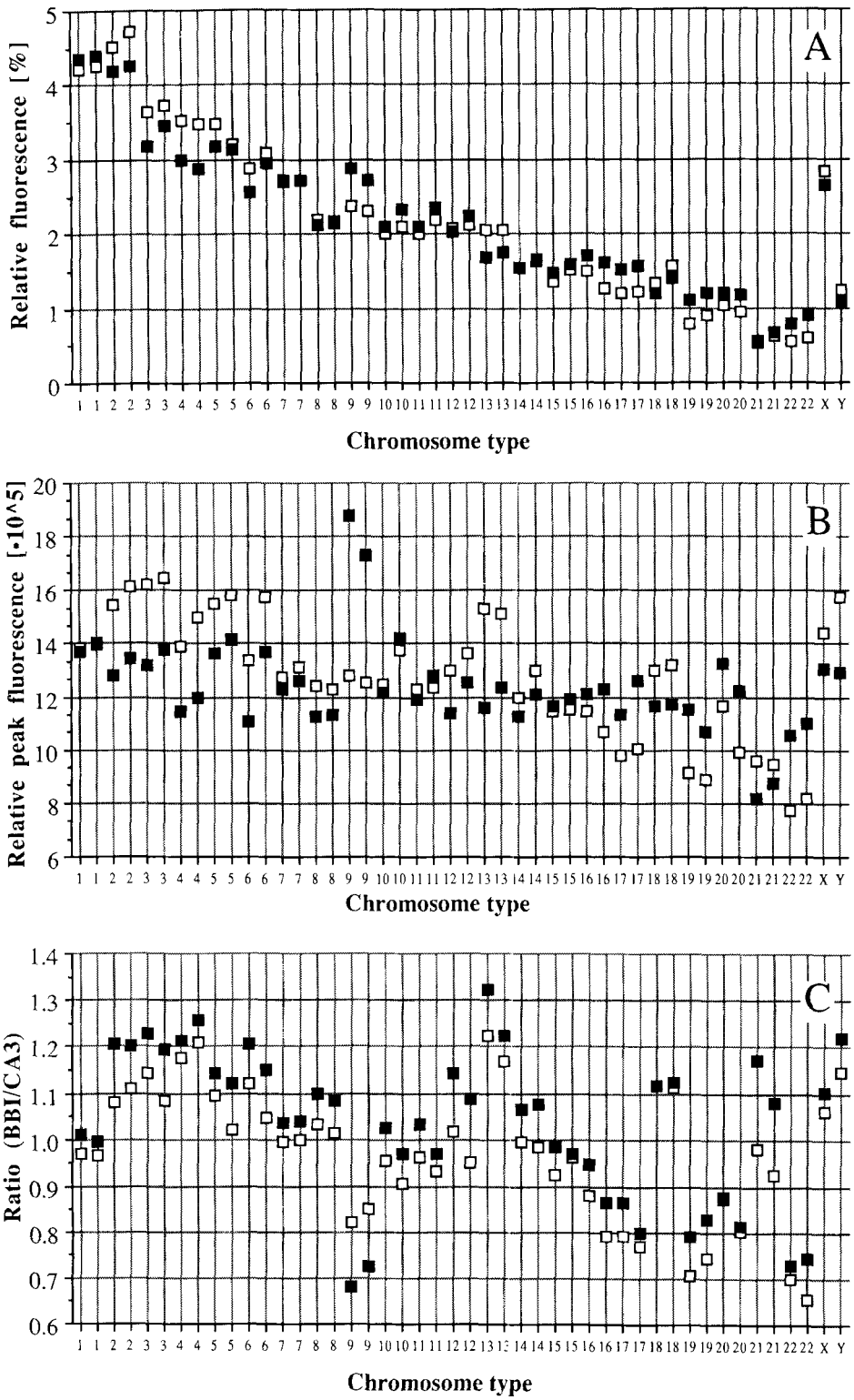

FIG. 4. Analyzed fluorescence intensity data for BBI and CA3 images correlated to the chromosome assignment. Measurements with the 63× objective (file: s13233). **A–C** as in Figure 3.

values can be assigned to many chromosomes. For example, those with large satellite sequences such as 9 and 13 exhibit extremes (low and high, respectively) in the ratio of the peaks, implying that such ratio functions might be particularly useful for distinguishing homolog variations in individuals. One should note that perfect registration between the two images is not required for the implementation of this method of analysis (as opposed to the use of ratios or logical operations on a pixel-by-pixel basis).

Bivariate and Multivariate Intensity Distributions

By constructing correlated plots of the intensity functions described in the previous section a resolution of almost the entire karyotype is achieved. The normalized total emissions for each chromosome, $S_{1,k}$ and $S_{2,k}$, can be plotted as a bivariate distribution familiar from flow karyotyping data with BBI on the Y axis and CA3 on the X axis. We show, for comparison, data from the same two metaphase plates given above (panels A of Figs. 5 and 6, respectively), and an additional plate imaged with the 40× objective in Figure 7A. The chromosome assignments for Figures 5 and 6 were determined by visual karyotyping of the images as stated above. The images for Figure 7 corresponded to a very condensed metaphase plate in which very few chromosomes could be unambiguously assigned by visual inspection. However, in view of the reproducibility of all the bivariate and multivariate distributions for the 40× images analyzed, we made the chromosome assignment by analogy to Figure 5.

The resolution of the chromosomes in the bivariate plots (panels A) is comparable to that achieved by quantitative flow karyotyping with good agreement for all chromosome assignments. We note, however, that the analogy is not exact since flow cytometric procedures measure randomized suspensions of chromosomes whereas in the microscope the chromosomes are preserved as sets corresponding to single cells.

The bivariate karyotype contains several groups of chromosomes which are not fully resolved (numbers 9–12, 14,15). The distinctive values associated with ratio functions of the intensities and peak values (panels C of Figs. 3, 4) suggested that certain multivariate plots could lead to improved resolution. Such is the case, as shown in panels B of Figures 5–7, in which the BBI intensity, $S_{1,k}$, of each chromosome is plotted on the Y axis and the ratio of the total emissions, $S_{1,k}/S_{2,k}$, is plotted on the X axis. Much better resolution of the large chromosomes 1–4, the numbers 13–16, the Y, and 21 is achieved than with the simple bivariate intensity distribution. A complementary display plotting the ratio of the maximum peaks, $M_{1,k}/M_{2,k}$, on the X axis (panels C of Figs. 5–7), resolves the X and considerably improves the resolution of the 9–12 chromosomes, a region which is notoriously difficult to resolve in flow karyotyping. (Chromosomes 10 and 11 were not resolved in the multivariate plots corresponding to the karyotypes which were assigned directly in Figs. 5 and 6. Therefore, we did not uniquely assign their positions in other spreads analyzed, e.g., Fig. 7, although the impression is that resolution into distinct pairs had been achieved.) These data show that the fluorescence intensity parameters determined from FDIM measurements may in themselves supply sufficient information for resolving all but possibly two chromosomes in the human karyotype.

Correlation Between Fluorescence and Absorbance Measurements of Metaphase Chromosomes

Having opposite base specificity, the DNA dyes BBI (A·T specific) and CA3 (G·C specific) do not compete for DNA binding sites. This is the basis of the utility of the bivariate distribution plot in which chromosomes of similar DNA content can be resolved by their differential staining by one or the other of the dyes. One would anticipate that the mean combined relative fluorescence intensity of both fluorophores for each chromosome would be a good measure of the relative DNA content of that chromosome. We have established this relationship by correlating the data obtained by flow analysis (Table 1 in ref. 14) and by ultraviolet absorption (Table 3 in ref. 27), in both cases determined as the means of numerous individuals and by use of autosomal normalization. Thus, a plot of the published values for individual (or in some cases groups of) chromosomes in the form of (1/2)[BBI + CA3 intensities] vs. the corresponding total OD units yielded a regression line with an intercept (fluorescence) of 0.052, a slope of 0.979, and a multiple correlation coefficient of 0.999. The fluorescence data in Figures 5A and 6A are plotted in Figure 8A,B against the standard published absorbance calibration (27). The correlations are good both in terms of the absolute values and the linear relationship, the deviations probably reflecting the properties of the individual karyotype used in our study. Taken together, these data reconfirm the utility of precise DNA content measurement for simple resolution of much of the human karyotype and show that such measurements can be achieved with fluorescence images from chromosome spreads using a digital imaging system.

DISCUSSION

Latt and coworkers demonstrated the A·T specific binding of BBI dyes and their utility for microscopic and flow cytometric measurements. Both Sahar and Latt (29) and Langlois and Jensen (17) showed that when combined, BBI and chromomycin A_3 complement each other due to their differential basepair selectivity in binding to mammalian DNA, and they also found that energy transfer occurred between the dyes on chromatin, chromosomes, and nuclei. This particular dye pair has been most successful in its extension to flow cytometry for karyotyping (12). However, the peaks in the flow karyotype overlap to some extent, influenced greatly by the quality of the chromosome

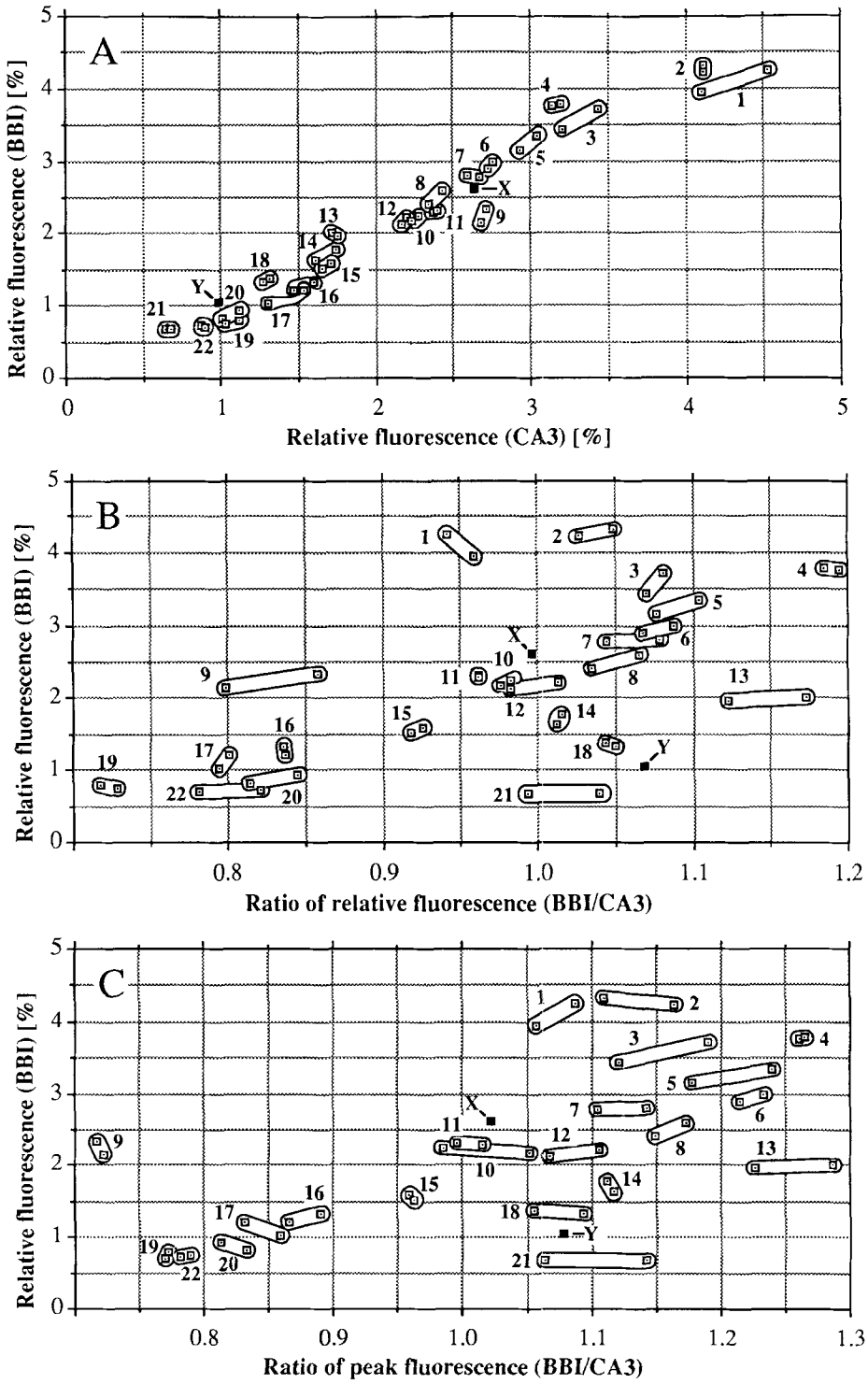

FIG. 5. Bivariate and multivariate karyotypes. Measurements with the 40× objective (Figs. 1, 2). **A:** Bivariate karyotype. Relative BBI fluorescence, $S_{1,k}$, plotted on the Y axis and relative CA3 fluorescence, $S_{2,k}$, plotted on the X axis. Homolog pairs are circled and chromosome numbers assigned by visual karyotyping (see text). **B:** Multivariate karyotype using the ratio of the relative fluorescence. The Y axis is the relative BBI fluorescence $S_{1,k}$, and the X axis the ratio $S_{1,k}/S_{2,k}$. **C:** Multivariate karyotype using the ratio of the peak fluorescence as a function. The Y axis is the relative BBI fluorescence, $S_{1,k}$, and the X axis the ratio $M_{1,k}/M_{2,k}$.

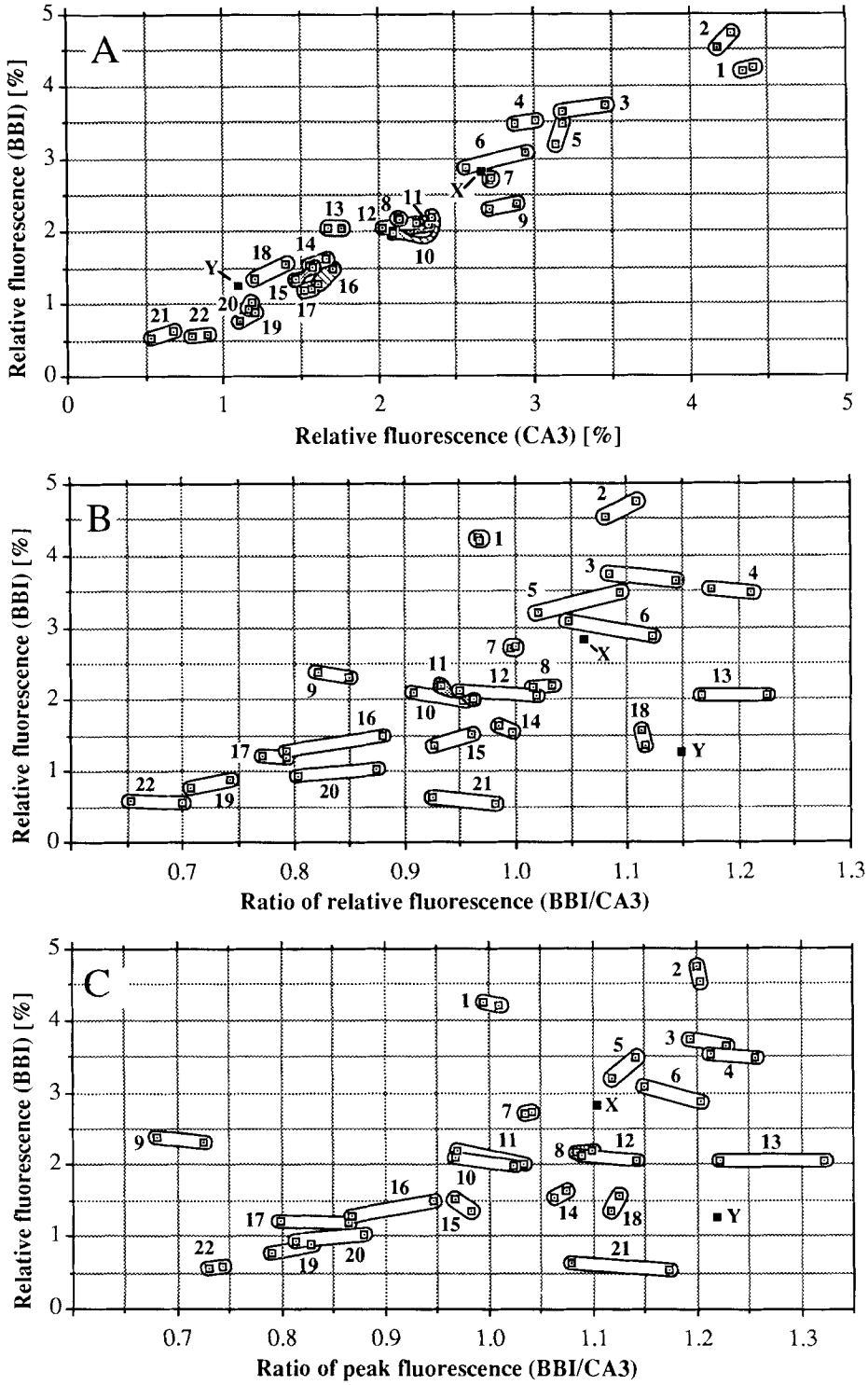

FIG. 6. Bivariate and multivariate karyotypes. Measurements with the 63× objective (file: s13233; Fig. 4). **A–C** as in Figure 5.

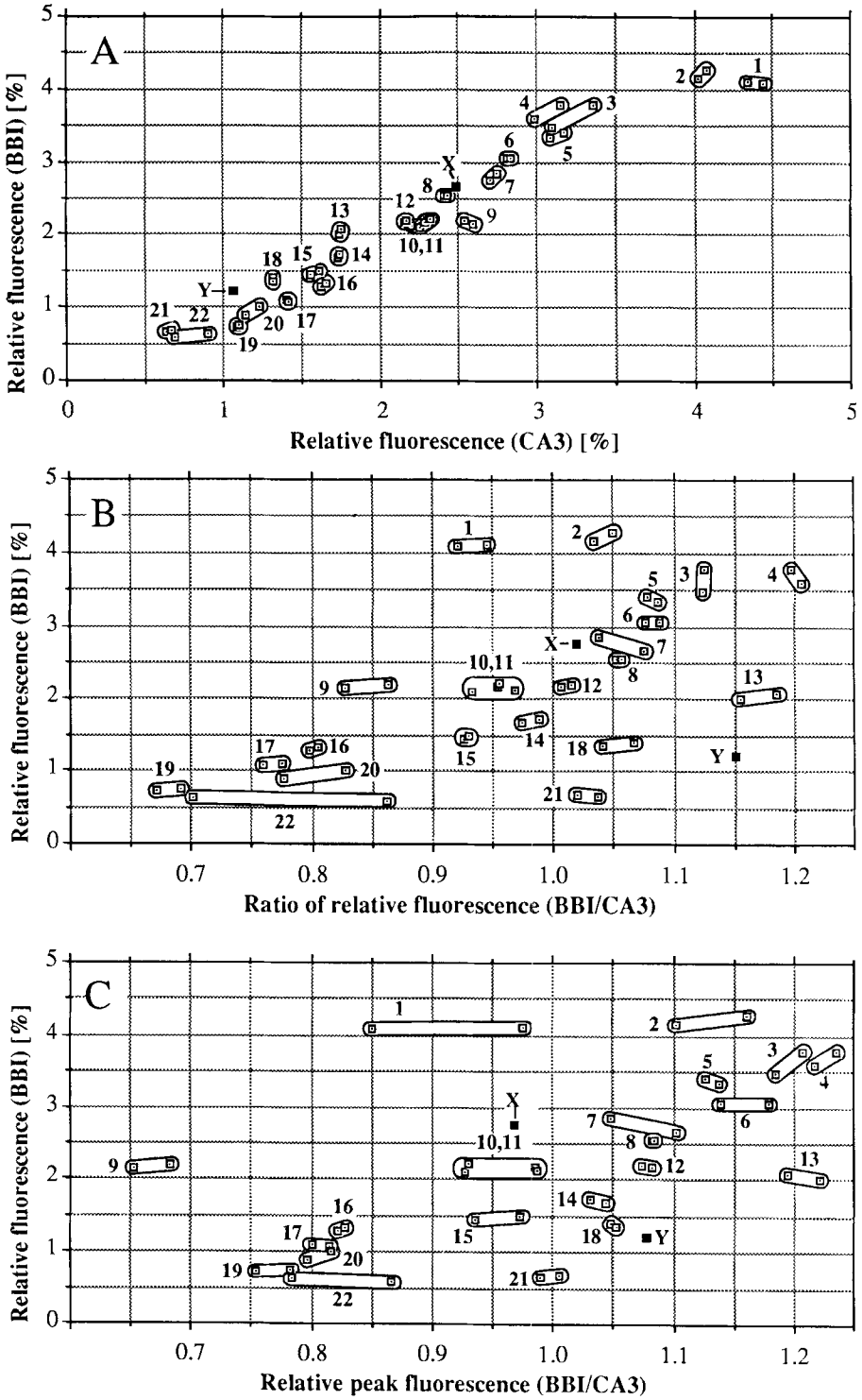

FIG. 7. Bivariate and multivariate karyotypes. Measurements with the 40× objective (file: s11213). **A–C** as in Figure 5. Chromosome assignments made by analogy to Figure 5 (see text).

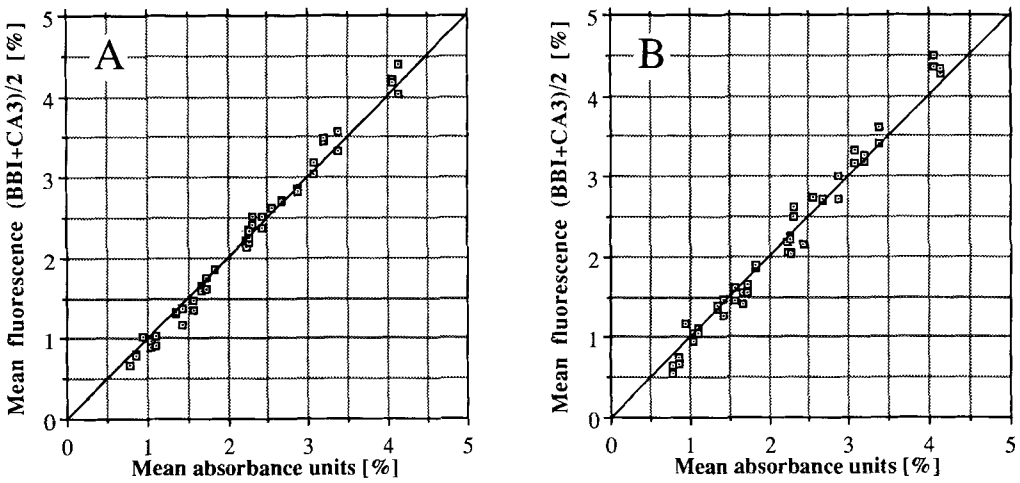

FIG. 8. Correlation of DNA content for the human karyotype determined from fluorescence and absorption measurements. The mean relative fluorescence of each chromosome, i.e., the average of the BBI and CA3 intensities, $(1/2)[S_{1,k} + S_{2,k}]$, is plotted on the Y axis against the data from Mayall et al. (Table 3 in ref. 27) for the mean relative OD of each chromosome on the X axis, renormalized to the full male karyotype. **A** and **B** correspond to the data in Figures 3 and 4, respectively.

suspension, the narrowness of the sample stream, and the intensity of the laser source. In order to use a bivariant distribution to detect chromosome abnormalities, the location, volume and width of the individual distributions must be determined. This procedure has limitations, particularly with respect to estimation of the background contribution (12), which restricts the utility of flow karyotyping to extensive abnormalities such as certain trisomies and translocations.

In this report we have shown that multivariate karyotyping can be achieved from fluorescence microscope images of chromosome spreads with resolution comparable to that of flow karyotypes without the necessity of analyzing banding patterns (Figs. 3–7). We believe it is essential that a linear fluorescence detector with high dynamic range and very low noise level, such as a scientific CCD camera, be used for these measurements in which one must distinguish chromosomes with differences in DNA content of a few femtograms (27). However, we have been able to analyze our data after normalization to 8 bits without significant degradation of the parameters. This suggests that it might be possible to achieve similar results with a stable, low-noise, linear, high-resolution video system.

The FDIM measurements derive a number of intensity parameters such as total intensity, maximum peak, and an intensity distribution function as well as shape and size of the chromosomes measured. Combinations of the intensity parameters into functions which are independent of chromosome condensation but which emphasize the differential staining of the two dyes, such as ratios of the intensities or ratios of the maximum peak, were found to be more powerful operators for karyotype resolution than the normalized integrated signals alone. The multivariate distributions shown in Figures 5–7, panels B, spread out chromosomes 1–4 and the 13–16 group as well as isolating the Y and 21. A complementary function using the ratio of the intensity maxima spreads out the 9–12 group (panels C) and would be expected to be very sensitive to individual polymorphisms in the karyotype. For example, the individual from whom the metaphase speads used in this study were derived has a pronounced G-C rich polymorphic region at the centromere of chromosome 9. The use of all three types of plots enables us to separate all but two chromosomes in the human karyotype from FDIM data using a simple Hg-arc excitation source and a CCD camera.

FDIM measurements appear to be rather insensitive to chromosome condensation or compaction, in contrast to those obtained by flow karyotyping or banding analyses. Chromosome spreads on a single slide can vary over fivefold in their extent of condensation, and we analyzed a range of such spreads. In this study we report measurements at two different microscope magnifications. In order to compare these data we calculated the cumulative intensities of each chromosome spread, typically $>10^7$ counts in our system, and expressed the individual chromosomes and other factors as percentages or fractions thereof. The reproducibility of any functional plot using this normalization procedure is shown in Figures 3 and 4 and is seen in the other plots as well. The 63× images we analyzed had as many as 1,700 pixels for the large chromosomes and as few as 150 for the small ones with a maximal pixel intensity of 8,000. The 40× images contained 40 pixels for the smallest chromosomes and up to 400 pixels for the largest with peak pixel intensities of 12,000. We have found that the images from the 40× objective gave highly consistent multivariate distributions, whereas the 63× images were not reproducible, a problem probably related to the small depth of field of the objective.

To achieve a measure of total DNA, the fluorescence must be uniformly excited and collected from all parts of each chromosome. The depth of field is much greater for the 40× NA 0.9 objective than for the 63× NA 1.3 objective, and we found that the analyses were not dependent on the exact focus at the lower magnification. In addition, although karyotyping by banding analysis requires long, less-condensed chromosomes, we find that very condensed chromosome plates give multivariate distributions with the least variation between homologs. The present CCD camera has 23 μm^2 pixels. Some newer scientific CCD sensors have considerably smaller pixels, which would increase the spatial resolution in the images obtained with the low magnification objectives.

In this initial report, we restricted our analysis to the chromosome sets of a single individual. However, the results suffice to indicate that with only a few cells an almost complete karyotype can be achieved on the basis of the multivariate fluorescence distributions alone. Further studies are in progress to determine the reproducibility and statistical validation of this technique and its potential resolving power in the analysis of abnormal karyotypes. The pioneering work of Latt on the use of combinations of dyes for enhanced banding and differentiation of particular chromosomes suggest that simultaneous determinations of DNA content and a banding profile derived from the emission at another wavelength could provide additional discrimination. The data presented here for the BBI-CA3 dye pair substantiate this expectation, as do preliminary results with other staining protocols. Simple digital imaging filtering techniques (e.g., Laplace, shown in Figs. 1, 2) enhance the weak banding patterns of the combined BBI and CA3 and could be used with more sophisticated digital imaging processing to derive banding profiles. Among the more difficult tasks for automated banding analysis for karyotyping using absorption measurements are segmentation and centromere identification (28). These problems are less severe in the case of the relatively more uniform fluorescence images. We are presently investigating the possible combination of FDIM karyotyping with in situ hybridization using specific DNA probes.

Several of the multivariate intensity distribution functions we have derived here could be used in flow karyotyping as easily as in FDIM since both peak and integral signals can be measured in most flow systems (although they may be subject to systematic distortion by convolution due to the finite size of the measuring aperture; 10). Slit illumination or a tightly focused laser beam would be required. Thus, it may be possible with a combination of the multivariate distributions to resolve and sort chromosomes which heretofore have been grouped in the bivariate karyotype (e.g. 9–12) or have been difficult to sort with high purity due to overlapping contiguous domains.

We conclude by acknowledging the personal stimulation derived from Sam Latt's unusually broad range of research expertise in biophysics and molecular biology. The many results and insights from his investigations of fundamental problems in human genetics have yet to be fully exploited. Sam Latt's passing represented a great loss to his colleagues and friends, but also left them with a clear challenge for the future.

ACKNOWLEDGMENTS

We thank C. Höfers for assistance in the banding karyotype analysis, Ellie Mann for help with the manuscript, and I.T. Young for constructive criticism.

LITERATURE CITED

1. Aikens RS, Agard DA, Sedat SW: Solid-state imagers for microscopy. Methods Cell Biol 29:291, 1989.
2. Arndt-Jovin DJ, Jovin TM: Analysis and sorting of living cells according to deoxyribonucleic acid content. J Histochem Cytochem 25:585, 1977.
3. Arndt-Jovin DJ, Jovin TM: Fluorescence labeling and microscopy of DNA. Methods Cell Biol 30:417, 1989.
4. Arndt-Jovin DJ, Latt SA, Striker G, Jovin TM: Fluorescence decay analysis in solution and in a microscope of DNA and chromosomes stained with quinacrine. J Histochem Cytochem 27:87, 1979.
5. Bartholdi MF, Meyne J, Johnston, RG, Cram LS: Chromosome banding analysis by slit-scan flow cytometry. Cytometry 10:124, 1989.
6. Brodie S, Giron J, Latt SA: Estimation of accessibility of DNA in chromatin from fluorescence measurements of electronic excitation energy transfer. Nature 253:470, 1975.
7. Carlson L, Caspersson T, Foley GE, Kudynowski J., Lomakka G, Simonsson E, Soren L: The application of quantitative cytochemical techniques to the study of individual mammalian chromosomes. Exp Cell Res 31:589, 1963.
8. Carrano AV, Gray JW, Langlois RG, Burkhart-Schultz KJ, Van Dilla MA: Measurement and purification of human chromosomes by flow cytometry and sorting. Proc Natl Acad Sci USA 76:1382, 1979.
9. Caspersson T, Farber S, Foley GE, Kudynowski J, Modest EJ, Simonsson E, Wagh U, Zech L: Chemical differential along metaphase chromosomes. Exp Cell Res 49:219, 1968.
10. Cram, LS, Bartholdi, MF, Wheeless Jr LL, Gray JW: Morphological analysis by scanning flow cytometry. In: Flow Cytometry: Instrumentation and Data Analysis, van Dilla MA, Dean PN, Laerum OD, Melamed MR (eds). Academic Press, Orlando, Florida, 1985, pp 164–194.
11. Crissman HA, Ora MS, Steinkamp JA: Rapid staining methods for analysis of deoxyribonucleic acid and protein in mammalian cells. J Histochem Cytochem 24:64, 1976.
12. Dean PN, Kolla S, Van Dilla MA: Analysis of bivariate flow karyotypes. Cytometry 10:109, 1989.
13. Dittrich W, Göhde W: Impulse fluorometry with single cells in suspension. Z Naturforsch 24b:360, 1969.
14. Gray JW, Langlois RG: Chromosome classification and purification using flow cytometry and sorting. Annu Rev Biophys Chem 15:195, 1986.
15. Hiraoka Y, Sedat JW, Agard DA: The use of a charge-coupled device for quantitative optical microscopy of biological structures. Science 238:36, 1987.
16. Jovin TM, Arndt-Jovin DJ: Luminescence digital imaging microscopy. Annu Rev Biophys Biophys Chem 18:271, 1989.
17. Langlois RG, Jensen RH: Interactions between pairs of DNA-specific fluorescent stains bound to mammalian cells. J Histochem Cytochem 27:72, 1979.
18. Langlois RG, Yu LC, Gray JW, Carrano AV: Quantitative karyotyping of human chromosomes by dual beam flow cytometry. Proc Natl Acad Sci USA 79:7876, 1982.
19. Latt SA: Fluorescent probes of chromosome structure and replication. Can J Genet Cytol 19:603, 1977.

20. Latt SA: Microfluorometric detection of deoxyribonucleic acid replication in human metaphase chromosomes. Proc Natl Acad Sci USA 70:3395, 1973.
21. Latt SA: Optical studies of metaphase chromosomes. Annu Rev Biophys Bioeng 5:1, 1976.
22. Latt SA, Brodie S, Munroe SH: Optical studies of complexes of quinacrine with DNA and chromatin: implications for the fluorescence of cytological chromosome preparations. Chromosoma 49:17, 1974.
23. Latt SA, Sahar E, Eisenhard ME: Pairs of fluorescent dyes as probes of DNA and chromosomes. J Histochem Cytochem 27:65, 1979.
24. Latt SA, Sahar E, Eisenhard ME, Juergens LA: Interactions between pairs of DNA-binding dyes: results and implication for chromosome analysis. Cytometry 1:2, 1980.
25. Latt SA, Stetten G: Spectral studies on 33258 Hoechst and related bisbenzimidazole dyes useful for fluorescent detection of deoxyribonucleic acid synthesis. J Histochem Cytochem 24:24, 1976.
26. Latt SA, Wohleb J: Optical studies of the interaction of 33258 Hoechst with DNA chromatin, and metaphase chromosomes. Chromosoma 52:297, 1975.
27. Mayall BH, Carrano AV, Moore II DH, Ashworth LK, Bennett DE, Mendelsohn ML: The DNA-based human karyotype. Cytometry 5:376, 1984.
28. Piper J, Granum E: On fully automatic feature measurement for banded chromosome classification. Cytometry 10:242, 1989.
29. Sahar E, Latt SA: Enhancement of banding patterns in human metaphase chromosomes by energy transfer. Proc Natl Acad Sci USA 75:5650, 1978.
30. Schwarzacher HG, Wolf U: Methods in human cytogenetics. Springer, Berlin Heidelburg, New York, 1974.
31. Stöhr M: Double beam application in flow techniques and recent results. In: Proceedings of the Second International Symposium on Pulse-Cytophotometry, Göhde W, Schumann J, Büchner T. (eds). European Press, Ghent, 1976, pp. 39–45.
32. Young BD, Ferguson-Smith MA, Sillar R, Boyd E: High-resolution analysis of human peripheral lymphocyte chromosomes by flow cytometry. Proc Natl Acad Sci USA 78:7727, 1981.